POLITECNICO DI TORINO
Repository ISTITUZIONALE

Design and testing of a device for the characterization of gas transfer through soap films and measurement protocol based on color matching

(Article begins on next page)

11 February 2024

Design and testing of a device for the characterization of gas transfer through soap films and measurement protocol based on color matching

Gabriele Falciani [a],[1], Luca Bergamasco [a],[*],[1], Agnese Amati [b], Gijsbert Verdoes [c], Indraneel Sen [d], Sylvestre Bonnet [b], Eliodoro Chiavazzo [a],[*]

[a] *Department of Energy, Politecnico di Torino, Corso Duca degli Abruzzi 24, 10129 Turin, Italy*
[b] *Leiden Institute of Chemistry, Leiden University, 2333 CC Leiden, the Netherlands*
[c] *Leiden Institute of Physics, Leiden University, 2333 CA Leiden, the Netherlands*
[d] *Department of Chemistry, Ångström Laboratory, Uppsala University, 751 20 Uppsala, Sweden*

ARTICLE INFO

ABSTRACT

Soap films are interesting for their potential utilization as soft, self-assembled, self-healing and possibly recyclable membranes. The intrinsic possibility of tuning their properties, such as e.g. surface and bulk elasticity or permeability, via tailored chemistry makes them flexible enough for a wide range of physical-chemical applications. Here we introduce a novel device that can serve as a research platform for the detailed experimental characterization of the soap film permeability to gases. The design and manufacturing of the novel platform are discussed, along with a sample characterization protocol based on a color-matching procedure for dioxygen diffusion through typical soap films. The experimental data is compared with the results obtained from a numerical model, specifically developed for the problem, and good agreement is found. In perspective, the proposed platform can serve for the precise characterization of gas transfer properties of soap films made from different surfactant mixtures and in the presence of different gases.

1. Introduction

The scientific interest for the extraordinary properties of soap films has a long history, with the first systematic observations of the colors in soap bubbles dating back to as early as the late 17th century [1]. Since then, much progress has been made, and today most of the fundamental aspects regulating their general characteristics have been understood [2,3]. Nonetheless, the possibility to obtain soap films and foams from different underlying chemistry, e.g. from different surfactants, addition of polymers [4,5] or nano-particles [6], provides remarkable tuning opportunities on the one hand, and uncertainty on the resulting properties on the other [7,8]. Therefore, a detailed characterization still requires proper, case-by-case analysis.

The investigation of the permeability of soap films to gases has been pioneered several decades ago by Princen and co-workers [9–11], especially focusing on Newton black films [12–15]. Since then, a commonly adopted experimental set-up to measure gas transfer was based on the diminishing bubble method, where a bubble is let shrink under gas diffusion driven by Laplace pressure [9,16]. Alternative

methods are based on the displacement of a soap film in a sealed pipe [17–19] or on the measurement of the size of a bubble which is continuously filled with gas, known as *continuous inflow method* [20]. The analysis of gas diffusion across soap films is important to understand, for example, part of the foam drainage process [21–23]. In recent years soap films have seen an increasing interest, with particular focus on e.g. their permeability [24], self-healing [25] and electric [26] properties for potential applications to e.g. triboelectric nanogenerators [27] or gas separators [20]. Another relevant example of application has been recently introduced in the framework of the Sofia project [28], where soap films have been proposed as photo-reactive membranes for artificial photosynthesis [29].

Soap films, indeed, can be regarded as soft, tunable membranes made of a thin layer of bulk water, stabilized at the interface with air by two self-assembled monolayers of surfactants. The latter, if properly functionalized [30], can be envisioned as photo-reactive surfaces, for example, for the overall reduction of carbon dioxide into solar fuel [31,32]. In this view, a proper separation of the gaseous products of the photo-reaction is of major importance and, in perspective, the possibility

* Corresponding authors.
  E-mail addresses: luca.bergamasco@polito.it (L. Bergamasco), eliodoro.chiavazzo@polito.it (E. Chiavazzo).
[1] These two authors contributed equally to this work.

to monitor the evolution of the gas products resulting from the photochemical reactions across the soap film is key.

Motivated mainly by this latter application, although not only, in this work we introduce a device (or platform) for the detailed characterization of the permeability of soap films to gases. Particularly, we report on the design, realization and utilization of the platform, providing a sample characterization protocol. The selected test case targets dioxygen diffusion through soap films made from water-based solutions of different surfactants, at predefined concentration. The platform is designed to allow light exposure and visual inspection of the soap film during the experiment, which is particularly convenient to monitor the evolution of the soap film dynamics. Indeed, we show how the time evolution of the soap film thickness, which is a major controlling parameter on gas diffusion, can be obtained via a color-matching procedure on experimental videos. The acquired data on gas diffusion is compared with the results obtained from a numerical model, specifically developed for the purpose. The experimental and numerical results are found to be in good agreement, demonstrating the effectiveness of the proposed platform as a characterization device.

The paper is organized as follows. We first introduce the dedicated experimental platform for the characterization of gas diffusion in Section 2, along with the presentation of the color matching technique used for the experimental measurement of the film thickness and of the set-up of the numerical model for the simulations. The comparison between the experimental data and the modeling results, with their physical interpretation, are discussed in Section 3. Finally, the conclusions on the analysis are drawn, and an outlook on the perspective developments for the proposed device are reported.

2. Materials and methods

2.1. Design of the experimental platform

A dedicated platform for the experimental characterization of the soap film permeability to gases in controlled conditions has been specifically designed and manufactured. The platform consists of two cylindrical gas chambers, enclosed by metal covers and separated by a holed and removable frame, designed to host the soap film (Fig. 1, left). The exploded renderings of the lower and upper parts of the platform are shown in Fig. 1 (center) and (right), respectively. The following components are shown: (1) aluminum body, (2) magnet to seal the top and bottom covers, (3) stainless-steel fixing rod, (4) rubber seal, (5) polymethyl methacrylate (PMMA) transparent window, (6) retaining nut in aluminum, (7) gas inlet, (8) stainless steel sensor holder plate, (9) stainless steel sensor holder, (10) stainless steel screw, (11) adaptor to be chosen depending on the sensor. For the sake of completeness, a section drawing of the complete assembly of the platform is also reported in Fig. S1.

The two cylindrical metal covers present gas-tight custom connections for independent gas filling and/or purging (under pressure controlled conditions within the chambers) and for needle type gas sensors. The metal covers are sealed using magnets (realizing gas-tight compartments), and provided of a transparent glass window for visual inspection of the soap film during the experiments, its light irradiation and for e.g. spectroscopic measurements. The frames to host the soap film (see Fig. 1, left) have been manufactured using different materials (stainless steel and anodized aluminum), with different thickness and diameters of the central hole (see Fig. S2).

2.2. Thickness of the soap film

The thickness of the soap film is measured using thin film interference theory, which allows to infer the thickness based on the reflected colors by the soap film [33,34]. Thus, we first briefly review and discuss the most relevant aspects related to color vision for a proper interpretation of the experimental images.

The coloring of an object depends on its properties and on those of the physical source of light. For the latter, let us consider the general case of a spectral power distribution for a black body. According to Planck's radiation law, the spectral radiance is given by [35]

$$I_\lambda(\lambda, T) = \frac{2hc^2}{\lambda^5} \left[exp\left(\frac{hc}{\lambda k_B T}\right) - 1 \right]^{-1}, \tag{1}$$

where h is the Planck's constant, c the speed of light, λ the wavelength, k_B the Boltzmann's constant and T the absolute temperature. For natural sunlight conditions, a black body power spectrum at proper temperature (e.g. 5777 K) can be typically adopted, although different spectra may also be considered. For colorimetry, standard illuminants provided by the CIE should be used [36]. In this work, laboratory experiments are performed under white lighting conditions from a fluorescent lamp. This latter (Aura T5 Eco Saver) is a 4000 K color temperature triphosphor lamp, with a good color rendering index [35]. Thus, in this case, we adopt the spectral power distribution of the CIE F11 standard illuminant (see Fig. S3), which represents a triband fluorescent source with a correlated color temperature (CCT) of 4000 K [36]. Note that, since the analysis is based on the colors rather than on light intensity, the position of the lamp is not particularly important as long as the light source is approximately white [37].

The chromaticity of the object (or light source) can be defined according to the CIE 1931 color spaces, which relate the wavelengths in the visible part of the spectral power distribution to the perceived colors from the human eye [38]. Particularly, the red (R), green (G) and blue (B) components, which are those available in pixels from camera
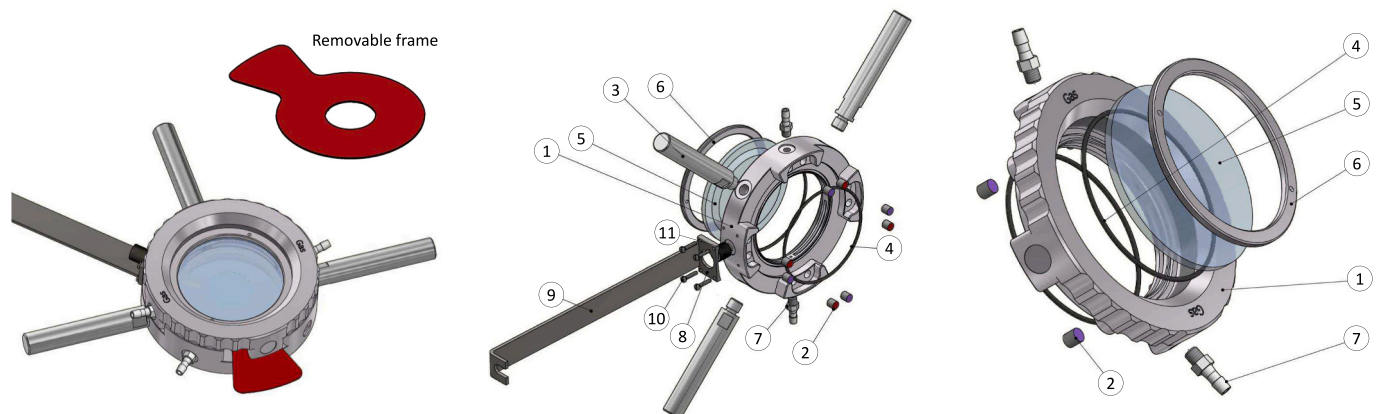

Fig. 1. Design of the experimental platform for the characterization of soap film permeability to gases: rendering of the complete assembly with the removable frame (shown in red) to host the soap film (left), exploded view of the lower (center) and upper (right) part of the platform. (For interpretation of the references to color in this figure legend, the reader is referred to the web version of this article.)

acquisitions, are formalized into a new set of primaries called X, Y and Z (also called tristimulus). Considering a discrete approximation of the spectral radiance $I_\lambda(\lambda)$, these primaries can be expressed as

$$X = k \sum_\lambda I_\lambda(\lambda) \overline{x}(\lambda) \Delta \lambda, \tag{2}$$

$$Y = k \sum_\lambda I_\lambda(\lambda) \overline{y}(\lambda) \Delta \lambda, \tag{3}$$

$$Z = k \sum_\lambda I_\lambda(\lambda) \overline{z}(\lambda) \Delta \lambda, \tag{4}$$

where $\overline{x}$, $\overline{y}$ and $\overline{z}$ stand for the color matching functions of the standard observer [35]. These latter functions are shown in Fig. S4. In the above equations, k is a normalization factor defined as

$$k = \left(\sum_\lambda I_\lambda(\lambda) \overline{y}(\lambda) \Delta \lambda \right)^{-1}, \tag{5}$$

and the sum is defined over the entire visible spectrum (here we consider 380–780 nm wavelengths). For a reflected color stimulus, I_λ in Eqs. 2, 3 and 4 is substituted by $\phi_\lambda(\lambda) = R_\lambda(\lambda) I_\lambda(\lambda)$, with $R_\lambda(\lambda)$ being the spectral reflectance factor or spectral reflectance [35]. For a soap film, the reflectance is calculated as [37]

$$R_\lambda(\lambda) = R_s^2 \frac{1 - \cos\varphi}{1 + R_s^4 - 2R_s^2\cos\varphi} + R_p^2 \frac{1 - \cos\varphi}{1 + R_p^4 - 2R_p^2\cos\varphi}, \tag{6}$$

with R_s and R_p being respectively the perpendicular and parallel reflection coefficients with respect to the incidence plane, and φ the phase difference between the reflected waves [37]. In this case, the reflection coefficients yield as

$$R_s = \frac{\cos\theta - (n^2 - \sin^2\theta)^{1/2}}{\cos\theta + (n^2 - \sin^2\theta)^{1/2}}, \tag{7}$$

$$R_p = \frac{n^2\cos\theta - (n^2 - \sin^2\theta)^{1/2}}{n^2\cos\theta + (n^2 - \sin^2\theta)^{1/2}}, \tag{8}$$

being θ the angle defined in Fig. 2 and n the index of refraction of the soap film (here assumed equal to that of water, $n = 1.33$). The
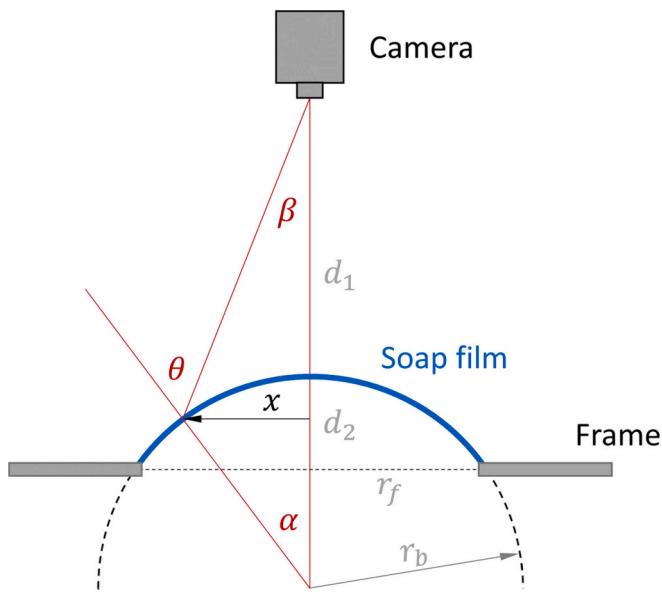

Fig. 2. Schematic representation of the experimental set-up, where the soap film evolution is recorded using a camera. The schematics refers to the general situation where the soap film can be curved under pressure effects [37].

Figure refers to the general situation where a soap film can be curved under the effect of pressure, and any position on the soap film can be identified via the angle $\theta = \alpha + \beta$, with analytical expressions for α, β and r_b as a function of the radius of the frame (r_f), distance of the camera (d_1), height of the soap film (d_2) and distance of the considered point on the soap film from the vertical axis of the hole (x) reported in [37]. The case of flat soap film within the frame is recovered when $d_2 \to 0$, for which $r_b \to \infty$ and thus $\alpha \to 0°$. In this situation, the angle θ depends only on β, that is, on the distance of the camera from the frame (d_1). In our case, the camera is positioned at approximately 10 cm above the frame, and the soap film is expected to experience a curvature under the effect of gas diffusion; therefore, in the following analyses, we will conservatively assume that in our set-up the angle θ can vary between 0° and 60° (see Fig. S5 for details).

The phase difference between the reflected waves is defined as [37]

$$\varphi = \frac{4\pi h}{\lambda} (n^2 - \sin^2\theta)^{1/2}, \tag{9}$$

with h being the thickness of the soap film. Finally, the X, Y and Z primaries are converted to the chromaticity coordinates of the CIE diagram as follows:

$$x = \frac{X}{X + Y + Z}, \tag{10}$$

$$y = \frac{Y}{X + Y + Z}, \tag{11}$$

$$z = \frac{Z}{X + Y + Z}. \tag{12}$$

Fig. 3 shows the analysis for $\theta = 0°$ and CIE F11 standard illuminant [36]. The figure shows the trajectory of the soap films for thickness ranging from 20 to 1480 nm on the CIE diagram (left) and the reflected colors as a function of the film thickness (right). The same analysis is reported also for $\theta = 30°$ and $\theta = 60°$ in Fig. S6 and S7, respectively. These latter two cases are representative of an intermediate and maximum value that the angle θ is expected to possibly assume in our set-up (see Fig. S5 for details).

When the film thickness is, typically, below 120–150 nm, the perceived color is silvery grey. When the thickness ranges 30–50 nm, soap films are called common black films, when the thickness is around 5 nm (which is close to the minimum thickness) they are called Newton black films [2]. On the other hand, very thick films (typically above 1000 nm) are perceived as transparent. In such cases, the thickness cannot be therefore any more inferred from thin film interference theory, and alternate techniques should be adopted. One possible technique relies on the analysis of the retraction speed during the film bursting. The opening velocity v_o is indeed related to the surface tension σ, density ρ and thickness h of the soap film as [39]:

$$v_o = \sqrt{\frac{2\sigma}{\rho h}}. \tag{13}$$

Thus, experimental acquisition of the opening velocity (e.g. using a high-speed camera) during bursting allows to obtain a measure of the film thickness based on characteristic values of the surface tension and density of the soap film. Finally, the combination of thin film interference theory and of the analysis of the retraction speed during bursting provide the means for a complete characterization of the soap film thickness over the relevant range for our purposes.

2.3. Numerical model

A continuum model representation is adopted for the transport of the gaseous molecules across the soap film. We adopt Fickian diffusion to describe the transport of gases in the gas phase and across the soap film,

as proposed by Princen and co-workers [9,10]. Subject to a concentration difference $(c_1 - c_2)$ in mol m^{-3}, the net molar flux of the gaseous species across the soap film can be defined as

$$\frac{dN}{dt} = kA(c_1 - c_2),$$ (14)

being N [mol] the diffusing gas moles, A [m^2] the area of the exposed surface of the soap film and k [m s^{-1}] the soap film permeability. This latter permeability can be defined as

$$k = H\left(\frac{2}{k_{ML}} + \frac{h}{D_w}\right)^{-1},$$ (15)

where H (dimensionless) is the Henry's law constant, k_{ML} [m s^{-1}] the permeability of the monolayers, h [m] the thickness of the water core and D_w [m^2 s^{-1}] the diffusion coefficient of the considered gas in bulk water. In this case, k_{ML} is an effective permeability, which encompasses the microscopic interactions among the surfactants within the monolayer at the air-water interface [24,40]. The overall permeability k can be physically interpreted as a resistance to gas diffusion, owing to the two monolayers and the water bulk.

In order to save computational time, we consider a 2D axial symmetric domain for the numerical model (see Fig. S8). The upper compartment is initially filled with an O$_2$-N$_2$ mixture (21%–79%, respectively) at ambient pressure. The lower chamber is initially filled by N$_2$ (100%), at ambient pressure. The system is gas-tight, and the two domains (upper and lower chambers) communicate only due to gas diffusion across the permeable soap film membrane. The 2D mesh adopted to solve the species diffusion equation is reported in Fig. S9. Flux continuity between the two domains is adopted as a boundary condition for the soap film. During the simulation, the partial pressure of O$_2$ in the lower chamber is measured using a probe on the internal side of the platform, to mimic the experimental setup (see Fig. S8). The gas diffusion flux is analyzed as a function of the soap film thickness, which is made varying in time according to the experimental values obtained from the color matching analysis [41].

3. Results and discussion

3.1. Testing of the experimental platform

The experimental platform presented in Section 2 is tested for the characterization of soap film permeability in typical conditions of

interest. The complete platform (see Fig. 4, left) is fixed on a precision support (black, holed plate in Fig. 4, right) via a specifically-designed three-point metal support, which allows to fine tune the horizontality of the platform, and thus, that of the soap film. The modular design allows integration of temperature, pressure and gas sensors.

The experimental protocol is performed according to the following procedure. First, a solution of water and the stock target surfactant is prepared at a given molar concentration; then, 70 μL of the surfactant solution are deposited on the holed metal frame and a plastic card is swiped over the frame to obtain the soap film (having care of avoiding any remaining liquid excess or droplet formation on the frame). Here, tests are performed using the 25 mm diameter, 0.5 mm thickness frame (see Fig. S2). The top and bottom covers are sealed, and connections between the chambers removed (see also Fig. S10), so that gas diffusion between the two compartments be only possible through the soap film. The two chambers can be finally filled with the target gases, by complete purging of air thanks to dedicated valves. In this case, we retain air in the upper chamber, whereas dioxygen is completely purged by nitrogen in the lower chamber. Then, during the experimental test, the dioxygen concentration is measured in the lower chamber, and the soap film coloring and evolution monitored from the top transparent glass window (Fig. 4, right).

3.2. Gas diffusion

The experimental gas diffusion was characterized for dioxygen in soap films realized using different surfactants at a predefined concentration. Particularly, a non-ionic surfactant (C$_{12}$E$_6$, hexaethylene glycol monododecyl ether from Sigma-Aldrich), an anionic surfactant (SDS, sodium dodecyl sulfate from Sigma-Aldrich), and a cationic surfactant (CTAB, hexadecyltrimethylammonium bromide from Sigma-Aldrich) were considered. The critical micelle concentration (CMC), that is, the concentration at which micellar aggregates are expected to start forming, for the three different surfactants is around 70 μM, 8 mM and 1 mM for C$_{12}$E$_6$, SDS and CTAB respectively [8]. The soap films were generated at 10 CMC concentrations of the bulk solutions in water. Note that no additional stabilizing products (e.g. glycerin) were added to prolong the lifetime of the soap films, so that the obtained stability and lifetime before bursting results from the base surfactants only.

For each analyzed case, the soap film was first generated (according to the described protocol) and the platform closed. The upper chamber was kept filled with ambient air (79% nitrogen and 21% dioxygen), whereas in the bottom chamber of the platform the dioxygen was
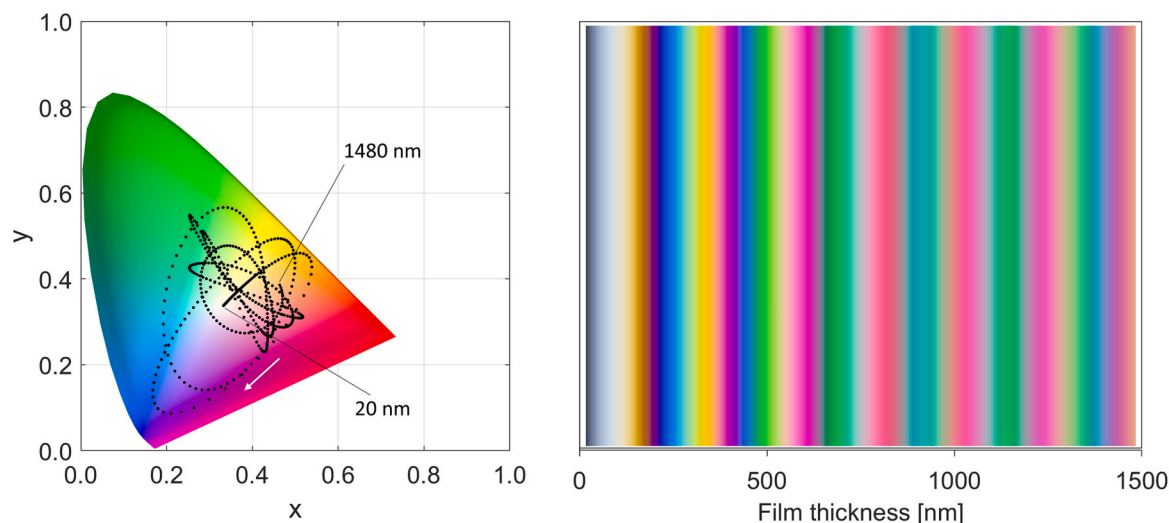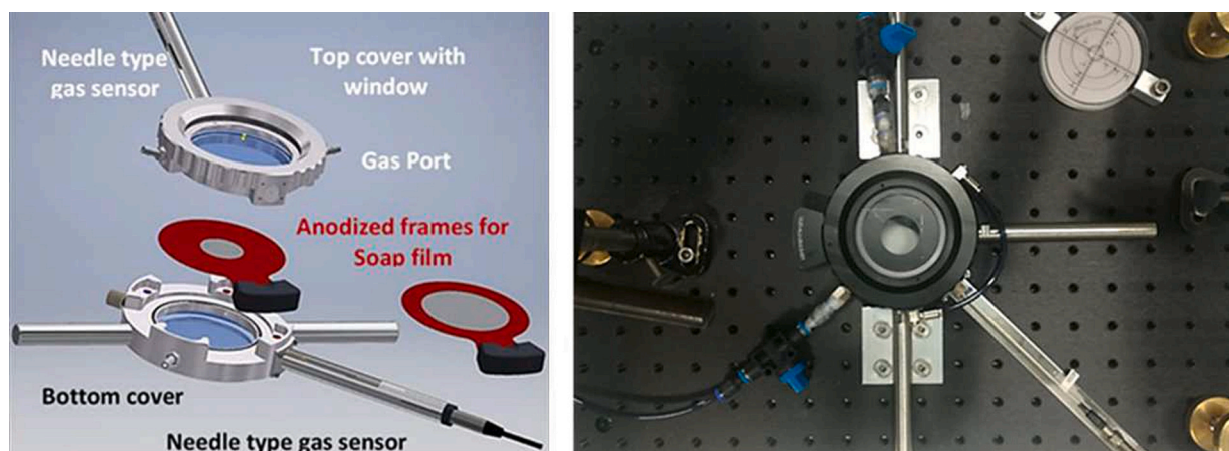

Fig. 3. Color analysis for $\theta = 0°$ in Fig. 2 and CIE F11 standard illuminant [36]. Chromaticity coordinates in the CIE diagram for soap films with thickness ranging from 20 nm to 1480 nm (left). Colors of the soap films as a function of the thickness (right).

Fig. 4. Experimental platform for the characterization of the soap film permeability to gases: exploded rendering of the different components of the platform (left), and the set-up of the manufactured product (right). Note that, for the experimental testing, the connection between the two chambers is removed so that gas diffusion between the two compartments be only possible through the soap film (see also Fig. S10).

completely purged with nitrogen (resulting in a ~100% atmosphere of this latter). After this preparation stage, the gas valve for purging the dioxygen was closed, and the experiment started. The dioxygen evolution in the lower chamber was then monitored using a dioxygen sensor (NeoFox, FOSPOR-R model), and the soap film coloring recorded using a camera.

The results obtained for the three different surfactants tested, namely SDS (left), $C_{12}E_6$ (center) and CTAB (right) at 10 CMC concentration are shown in Fig. 5. The solid red lines represent the average dioxygen evolution obtained from three experimental repetitions, and the red transparent band the related variance in the time span where no bursting of the soap film has been observed. On the other hand, the blue transparent area shows the region where the (earliest) bursting of the soap films has been observed during the repetitions of the experimental measurements. In such regions, the red dashed lines show the extrapolation of the dioxygen evolution dynamics according to best-fitting curves. These latter curves have the analytical form of the Gompertz function, namely

$$f(t) = aexp(-bexp(-ct)). \tag{16}$$

This analytical form has been chosen as it provides an adequate representation of the experimental data over the whole observed dynamics (see the raw experimental data for the three tests and the related best-fitting curves in Fig. S11).

During the experiment, two counteracting phenomena on the gas flow rate from one side to the other of the membrane occur. The permeability of the soap film increases due to its thinning; on the other hand, the concentration gradient across the film decreases due to diffusion. This competition results in a steep increase of the dioxygen concentration in the lower chamber during the first part of the experiment (where the film is thick and the concentration gradient is high), and in a flattening of the curve in the second part, where the concentration gradient becomes small. The time evolution dynamics of the dioxygen diffusion is similar for the three tested surfactants, whereas the soap films made from the CTAB surfactant are found to be the most stable (no bursting has been observed throughout the whole experiment in all tested cases). Soap films made from SDS and $C_{12}E_6$ show reduced stability, having a similar time span where bursting is observed.

3.3. Evolution of the soap film thickness

The evolution of the soap film coloring was recorded using a common camera, positioned on the top (view) of the soap film. The resulting video is processed using MATLAB®, to extract and analyze the target frames.

Fig. 6 shows the colors at different instants and the related dioxygen concentration acquired in the lower chamber during the experiment for the $C_{12}E_6$ surfactant at 10 CMC concentration. Based on the full set of
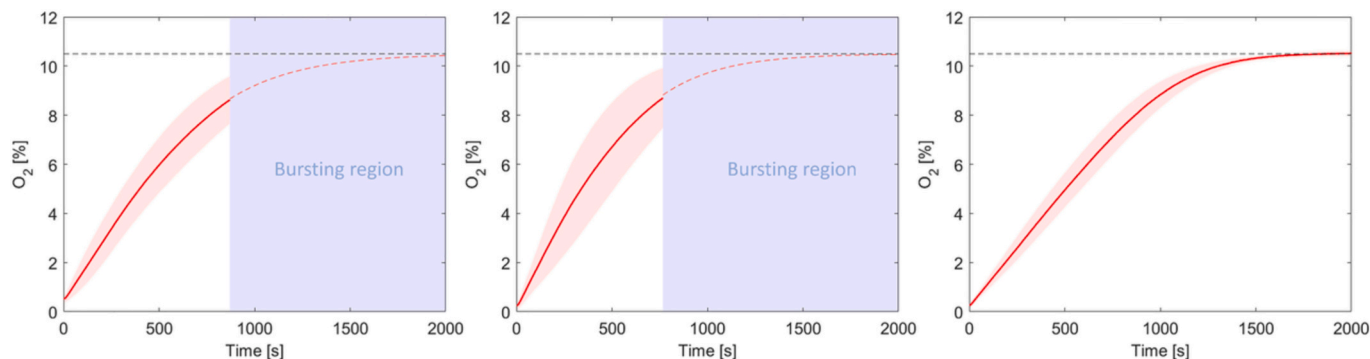
Fig. 5. Dioxygen evolution dynamics across the soap films made from the three tested surfactants, namely SDS (left), $C_{12}E_6$ (center) and CTAB (right) at 10 CMC concentration. The solid red lines correspond to the average of the experimental measurements (over three repetitions), and the red transparent band the related variance in the time span where no bursting of the soap film has been observed. The blue, transparent area indicates the region where bursting of the soap films has been observed during the experimental measurements. In those regions, the red dashed lines show the extrapolation of the dioxygen evolution dynamics according to best-fitting curves (Gompertz function). The black dashed line (at 10.5% dioxygen concentration) show the final expected condition. (For interpretation of the references to color in this figure legend, the reader is referred to the web version of this article.)
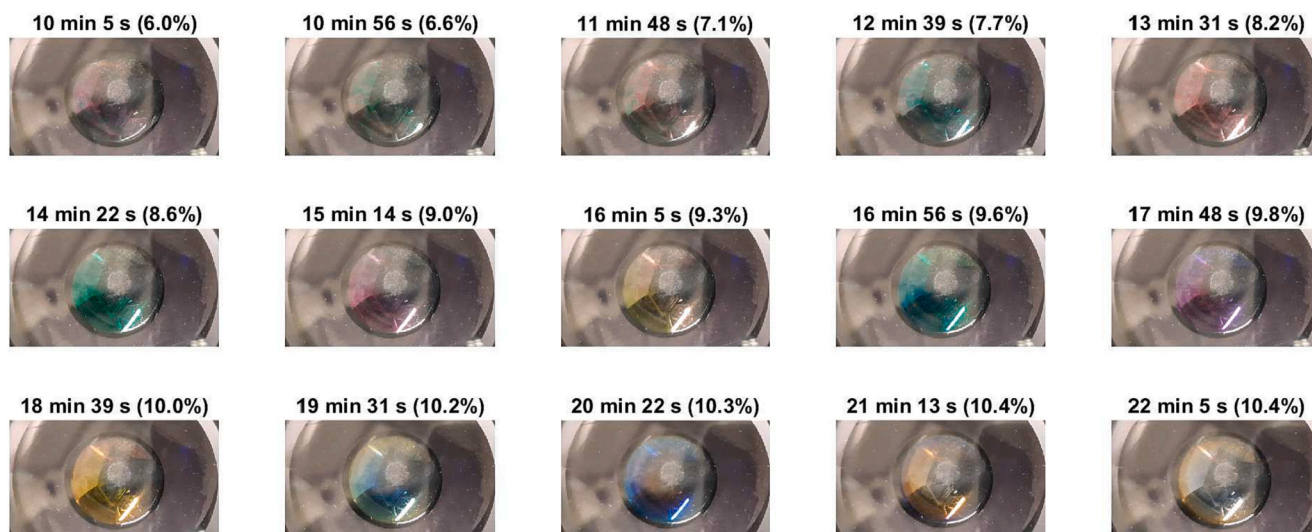
Fig. 6. Video frames of the soap film interference colors obtained during the experiment for the $C_{12}E_6$ surfactant at 10 CMC concentration. The measured O_2 concentration in correspondence of each frame is reported on top of each frame.

available video frames, the color of the soap film is automatically extracted via an analysis of the average pixel colors. This allows to obtain the time evolution of the soap film coloring. The results are shown in Fig. 7, where the experimental dioxygen evolution is compared with the soap film dynamics. During the dioxygen purging phase (A), the soap film is is very thick and transparent. After the experiment is started (2 min and 34 s in this test), the soap film remains substantially transparent (B) up to around 7 min. It then undergoes a rapidly-changing color phase (C) up to around 10 min, when color changing becomes smooth (D). Finally, the soap film bursting is observed close the final expected dioxygen concentration (E). The evolution of colors (D) can thus be used to infer the related thickness of the soap film, whereas for the initial thickness the analysis of the retraction speed during bursting is adopted. This latter analysis, performed using a speed camera at 960 fps (frames per second) for a soap film made from $C_{12}E_6$ surfactant at 10 CMC concentration (see Fig. S12), provided an estimate of the initial thickness ranging between 4.5 and 7.5 μm (assuming the liquid density is $\rho = 1000$ kg m^{-3} and the surface tension is $\sigma = 35$ mN m^{-1} in Eq. 13).
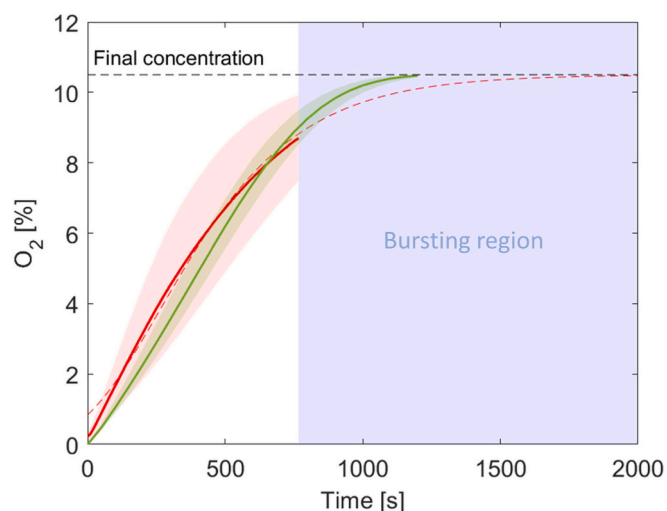
3.4. Model comparison

The overall soap film permeability in Eq. 15 is strongly affected by the soap film thickness. Thus, the numerical solution is obtained using the experimental thickness as an input for the continuum model. The thickness is obtained via color matching procedure on the experimental data. The evolution of colors in Fig. 7 is analyzed, and each color can be associated with the corresponding thickness (e.g. that reported in Fig. 3 for flat horizontal soap films and $\theta = 0°$). However, note that a curvature of the soap film is observed during the experiment (see video frames in Fig. 6) due to a small over-pressure in the bottom chamber; thus, the color-to-thickness conversion may be better approximated considering the effect of the curvature. To account for this effect, we extract the evolution of the thickness considering three cases for the angle θ in Fig. 2: $\theta = 0°$, $\theta = 30°$ and $\theta = 60°$. The latter two values are chosen as intermediate and maximum possible angles for our experiment (see Fig. S5), and the related color maps as a function of the thickness are shown in Fig. S6 and S7 respectively. Considering that the thickness is manually extracted based on the perceived color, we conservatively consider a $\pm20\%$ error on the reading for each examined diagram. This uncertainty corresponds to the maximum reading error on the thickness per each perceived color (i.e. the width of each color on the diagrams with respect to the average expected thickness). The numerical model is then run for all cases, using the values for the diffusion coefficients,

permeabilities and Henry's law constants reported in Table S1. The detailed results for all cases are shown in Fig. S13.

The average dioxygen dynamics is shown in Fig. 8, where the numerical result (green curve) is compared with the experimental data (red curve) for the $C_{12}E_6$ at 10 CMC concentration. As the figure shows, the numerical solution recovers the experimental curve with quite satisfactory accuracy (18% mean absolute percentage error). The slight discrepancy in the shapes of the two curves may be sought in the simplified representation adopted in the numerical model, where the thickness is assumed to be constant over the whole soap film (although time evolving). In the experiment, the thickness is expected to vary over the soap film, with the minimum value being reached at the top of the curved film due to liquid drainage. Although one such detailed mapping of the thickness over the soap film could not be achieved with the
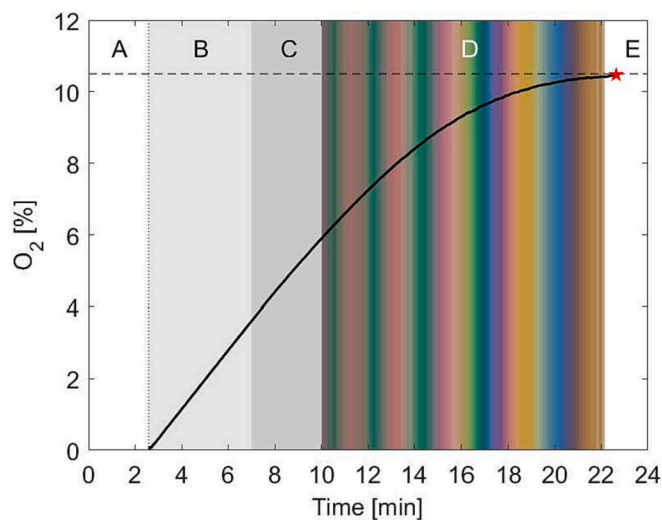
Fig. 7. Experimental dioxygen diffusion and related color patterns for the $C_{12}E_6$ surfactant at 10 CMC concentration. The reported time spans correspond to: dioxygen purging (A); transparent soap film (B); rapidly-changing colors (C); smooth color changing (D) and bursting of the soap film (E). The dioxygen data acquisition starts at 2 min 34 s. The horizontal dashed line indicates the final dioxygen concentration, expected at 10.5%. The red pentagram pinpoints the observed bursting condition of the soap film. (For interpretation of the references to color in this figure legend, the reader is referred to the web version of this article.)

Fig. 8. Comparison of the mean experimental data (red curve) and the modeling results (green curve) on the dioxygen diffusion dynamics for the $C_{12}E_6$ surfactant at 10 CMC concentration. (For interpretation of the references to color in this figure legend, the reader is referred to the web version of this article.)

current experimental set-up, the simplified representation adopted has proven reasonable accuracy.

4. Conclusions

A device for the experimental characterization of the soap film permeability to gases has been introduced, and the main aspects underlying its design and manufacturing presented and discussed.

The novel platform has been tested for a typical sample case, of dioxygen diffusion through soap films made from different surfactants at predefined concentration. The acquired data has been analyzed and interpreted via a combination of automated data extraction techniques and a modeling approach. Particularly, automated color extraction from the experimental videos has allowed to infer the time evolution of the soap film thinning during the experiment via thin-film interference theory. The missing information on the thickness in the transparent time spans have been complemented by an analysis of the soap film opening velocity via Taylor-Culick model. The obtained data on the evolution of the thickness has been used as an input to assess and validate a numerical model for gas diffusion through soap films. The experimental and numerical results on gas diffusion have been found to be in satisfactory agreement (18% mean absolute percentage error), considering the adopted simplified model. The agreement can be expected to improve using more detailed modeling representations.

The gas (here, dioxygen) diffusion has been found to have similar dynamics for the examined anionic, non-ionic and cationic surfactants, whereas the soap films made from these latter have been found to be the most stable among those tested. The considered conditions represent only a first validation test case for the introduced platform. In perspective, indeed, the developed framework could easily be used to test different gases (e.g. CO_2 and CO) and to explore a wider range of surfactant concentrations within the soap films, to characterize e.g. the effect of suspended agglomerates on the gas diffusion dynamics across soap films. Moreover, a tailored lighting set-up in combination with an automated system for acquisition of the color-to-thickness mapping, could serve for systematic characterization of e.g. liquid drainage, evaporation phenomena, or photo-reaction gas products under sunlight exposure.

CRediT authorship contribution statement

Gabriele Falciani: Conceptualization, Methodology, Software, Validation, Formal analysis, Writing – original draft, Writing – review & editing, Visualization. **Luca Bergamasco:** Conceptualization, Methodology, Software, Validation, Formal analysis, Writing – original draft, Writing – review & editing, Visualization. **Agnese Amati:** Investigation. **Gijsbert Verdoes:** Conceptualization, Visualization. **Indraneel Sen:** Conceptualization, Methodology, Project administration, Funding acquisition. **Sylvestre Bonnet:** Conceptualization, Methodology, Validation, Supervision, Project administration, Funding acquisition. **Eliodoro Chiavazzo:** Conceptualization, Methodology, Validation, Supervision, Project administration, Funding acquisition.

Declaration of Competing Interest

The authors declare that they have no known competing financial interests or personal relationships that could have appeared to influence the work reported in this paper.

Data availability

Data will be made available on request.

Appendix A. Supplementary data

Supplementary data to this article can be found online at https://doi.org/10.1016/j.icheatmasstransfer.2023.107161.

References

[1] G. Gochev, D. Platikanov, R. Miller, Chronicles of foam films, Adv. Colloid Interf. Sci. 233 (2016) 115–125.

[2] C. Isenberg, The Science of Soap Films and Soap Bubbles, Dover Publications, 1992.

[3] R.J. Pugh, Bubble and Foam Chemistry, Cambridge University Press, 2016.

[4] S. Frazier, X. Jiang, J.C. Burton, How to make a giant bubble, Phys. Rev. Fluids 5 (1) (2020), 013304.

[5] G. Gochev, Thin liquid films stabilized by polymers and polymer/surfactant mixtures, Curr. Opin. Colloid Interface Sci. 20 (2) (2015) 115–123.

[6] Z. AlYousef, M. Almobarky, D. Schechter, Enhancing the stability of foam by the use of nanoparticles, Energy Fuel 31 (10) (2017) 10620–10627.

[7] H. Manikantan, T.M. Squires, Surfactant dynamics: hidden variables controlling fluid flows, J. Fluid Mech. 892 (2020).

[8] M.J. Rosen, J.T. Kunjappu, Surfactants and Interfacial Phenomena, John Wiley & Sons, 2012.

[9] H. Princen, S. Mason, The permeability of soap films to gases, J. Colloid Sci. 20 (4) (1965) 353–375.

[10] H. Princen, J.T.G. Overbeek, S. Mason, The permeability of soap films to gases: II. A simple mechanism of monolayer permeability, J. Colloid Interface Sci. 24 (1) (1967) 125–130.

[11] G. Andreatta, L.-T. Lee, F.K. Lee, J.-J. Benattar, Gas permeability in polymer-and surfactant-stabilized bubble films, J. Phys. Chem. B 110 (39) (2006) 19537–19542.

[12] R. Krustev, D. Platikanov, M. Nedyalkov, Permeability of common black foam films to gas. Part 1, Colloids Surf. A Physicochem. Eng. Asp. 79 (1) (1993) 129–136.

[13] R. Krustev, D. Platikanov, M. Nedyalkov, Permeability of common black foam films to gas. Part 2, Colloids Surf. A Physicochem. Eng. Asp. 123 (1997) 383–390.

[14] R. Muruganathan, R. Krastev, H.-J. Müller, H. Möhwald, Foam films stabilized with dodecyl maltoside. 2. Film stability and gas permeability, Langmuir 22 (19) (2006) 7981–7985.

[15] M. Nedyalkov, R. Krustev, D. Kashchiev, D. Platikanov, D. Exerowa, Permeability of newtonian black foam films to gas, Colloid Polym. Sci. 266 (1988) 291–296.

[16] M. Ramanathan, H.-J. Müller, H. Möhwald, R. Krastev, Foam films as thin liquid gas separation membranes, ACS Appl. Mater. Interfaces 3 (3) (2011) 633–637.

[17] C. Hadji, B. Dollet, H. Bodiguel, W. Drenckhan, B. Coasne, E. Lorenceau, Impact of fluorocarbon gaseous environments on the permeability of foam films to air, Langmuir 36 (44) (2020) 13236–13243.

[18] P.N. Quoc, P.L. Zitha, P.K. Currie, Effect of foam films on gas diffusion, J. Colloid Interface Sci. 248 (2) (2002) 467–476.

[19] K. Sujatha, T. Das, R. Kumar, K. Gandhi, Permeation of gases through liquid films, Chem. Eng. Sci. 43 (6) (1988) 1261–1268.

[20] J. Reznickova, R. Petrychkovych, J. Vejrazka, K. Setnickova, P. Uchytil, Gas separation ability of the liquid bubble film, Sep. Purif. Technol. 166 (2016) 26–33.

[21] S. Tcholakova, Z. Mitrinova, K. Golemanov, N.D. Denkov, M. Vethamuthu, K. Ananthapadmanabhan, Control of ostwald ripening by using surfactants with high surface modulus, Langmuir 27 (24) (2011) 14807–14819.

[22] N. Denkov, S. Tcholakova, N. Politova-Brinkova, Physicochemical control of foam properties, Curr. Opin. Colloid Interface Sci. 50 (2020), 101376.

[23] Z. Briceño-Ahumada, D. Langevin, On the influence of surfactant on the coarsening of aqueous foams, Adv. Colloid Interf. Sci. 244 (2017) 124–131.

[24] G. Falciani, R. Franklin, A. Cagna, I. Sen, A. Hassanali, E. Chiavazzo, A multi-scale perspective of gas transport through soap-film membranes, Mol. Syst. Design Eng. 5 (5) (2020) 911–921.

[25] L. Courbin, H.A. Stone, Impact, puncturing, and the self-healing of soap films, Phys. Fluids 18 (9) (2006), 091105.

[26] R. Gera, H.J. Bakker, R. Franklin-Mergarejo, U.N. Morzan, G. Falciani, L. Bergamasco, J. Versluis, I. Sen, S. Dante, E. Chiavazzo, et al., Emergence of electric fields at the water–c12e6 surfactant interface, J. Am. Chem. Soc. 143 (37) (2021) 15103–15112.

[27] J. Nie, Z. Wang, Z. Ren, S. Li, X. Chen, Z. Lin Wang, Power generation from the interaction of a liquid droplet and a liquid membrane, Nat. Commun. 10 (1) (2019) 1–10.

[28] European Commission, EU H2020 FET-OPEN project Sofia (Soap Film based Artificial Photosynthesis), Available at: https://cordis.europa.eu/project/id/828838. Accessed on: 2022-09-26.

[29] A.F. Collings, C. Critchley, Artificial Photosynthesis: From Basic Biology to Industrial Application, John Wiley & Sons, 2007.

[30] H. Song, N. Kaul, A. Amati, G. Falciani, L. Bergamasco, C. van Rijn, E. Chiavazzo, I. Sen, S. Bonnet, L. Hammarström, Realizing symmetry-breaking architectures in soap films, Zenodo (2023), https://doi.org/10.5281/zenodo.8088199.

[31] G. Falciani, L. Bergamasco, S.A. Bonke, I. Sen, E. Chiavazzo, A novel concept of photosynthetic soft membranes: a numerical study, Discov. Nano 18 (1) (2023) 9.

[32] G. Falciani, E. Chiavazzo, An overview on modelling approaches for photochemical and photoelectrochemical solar fuels processes and technologies, Energy Convers. Manag. 292 (2023), 117366.

[33] C.V. Boys, Soap Bubbles, their Colours and the Forces which Mold them vol. 542, Courier Corporation, 1959.

[34] T.-S. Yang, C.-Y. Wen, C.-Y. Lin, Interpretation of color fringes in flowing soap films, Exp. Thermal Fluid Sci. 25 (3–4) (2001) 141–149.

[35] H.-C. Lee, Introduction to Color Imaging Science, Cambridge University Press, 2005.

[36] M.D. Fairchild, Color Appearance Models, John Wiley & Sons, 2013.

[37] Y. Afanasyev, G.T. Andrews, C. Deacon, Measuring soap bubble thickness with color matching, Am. J. Phys. 79 (10) (2011) 1079–1082.

[38] T. Smith, J. Guild, The cie colorimetric standards and their use, Trans. Opt. Soc. 33 (3) (1931) 73.

[39] J.-L. Pierson, J. Magnaudet, E.J. Soares, S. Popinet, Revisiting the Taylor-culick approximation: retraction of an axisymmetric filament, Phys. Rev. Fluids 5 (7) (2020), 073602.

[40] R. Farajzadeh, R. Krastev, P.L. Zitha, Foam film permeability: theory and experiment, Adv. Colloid Interf. Sci. 137 (1) (2008) 27–44.

[41] B. Mandracchia, Z. Wang, V. Ferraro, M.M. Villone, E. Di Maio, P.L. Maffettone, P. Ferraro, Quantitative imaging of the complexity in liquid bubbles' evolution reveals the dynamics of film retraction, Light: Sci. Appl. 8 (1) (2019) 20.